Progress In Electromagnetics Research C, Vol. 131, 145–158, 2023

A Novel Diagonally Symmetric Fractal Antenna with Wideband Characteristics for Internet of Things Applications

Geeta Kalkhambkar[1, *], Rajashri Khannai[2], and Pradeep Chindhi[1]

Abstract—The Internet of Things (IoT) has become a vital part of life, with an increasing number of connected devices; its small size and high data transmission rate have attracted the attention of many researchers. Antenna plays a significant role in providing wireless signal connectivity. This work proposes a third-level iterated diagonally symmetric fractal antenna with improved bandwidth for faster data transmission. A partial ground plane with a notch has been experimented to adjust the antenna impedance over a wider bandwidth parametrically. Based on surface current distribution, the antenna has been optimized to eliminate the stopband. Following optimization, a modal shift separated two overlapping modes and produced a new resonance close to the stopband. The proposed antenna covers IoT applications between 2 GHz and 7 GHz. The design has been simulated in mentor graphics and CST studio, and it is verified on a vector network analyser and in an anechoic chamber. The measured S_{11} and gain are in good agreement with the simulated results. The overall antenna size is 40 mm in length, 40 mm in width, and 1.6 mm in height, and it is fabricated on an FR-4 substrate with a dielectric constant of 4.4.

1. INTRODUCTION

The internet of things (IoT) is the future of device-to-device and person-to-person communication. IoT devices demand three major things from the manufacturer [1], as revealed in Figure 1 below.

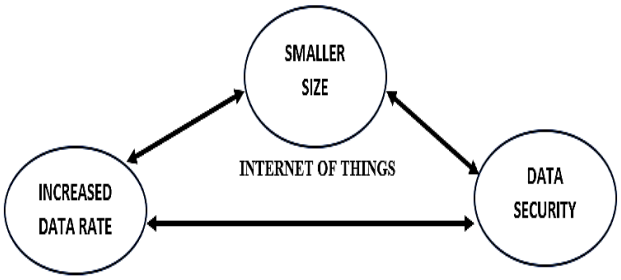

Figure 1. IoT device requirement.

A smaller antenna size is desired to reduce the overall size of an IoT device. Increased data rate requires wideband antennas. Achieving wider bandwidth with a smaller antenna size is challenging for IoT antenna designers. Planar antennas, such as microstrip antennas, are often the best for IoT antennas. With conventional design equations, it is impossible to achieve a smaller size and broader

Received 1 February 2023, Accepted 14 March 2023, Scheduled 24 March 2023
* Corresponding author: Geeta Kalkhambkar (geetakalkhambkar@gmail.com).
[1] Sant Gajanan Maharaj College of Engineering Mahagaon, India. [2] Department of Computer Science Engineering, KLE Dr. MSSCET, Belagavi, India.

bandwidth [2]. Narrow bandwidth is the disadvantage in the case of microstrip antennas. Fractal antennas are envisioned to increase the bandwidth with their self-similar and space-filling properties, which lead to increasing the current path without increasing the actual size of the antenna [3]. The research on fractal antennas started in 1991 [4, 5]. The area of fractal antennas still needs to be fully explored. Recently, many researchers have been working in the field of fractal antennas, and medical applications [6], multiple-input multiple-output (MIMO) [7, 8], IoT [8], and 5G [9, 10] are significant areas of research. Artificial neural network helps optimize the antenna for better performance with reduced size [11]. An improved polarization pattern can be obtained with a slotted ground plane and also helps the antenna to resonate at higher frequencies [12]. A defected ground structure and coplanar waveguide (CPW) feed can be incorporated to increase the antenna's bandwidth [13]. A hybrid fractal antenna with a Koch curve and mender line prompts higher-order modes to excite, giving a wider operating range of frequencies [14]. The modal study is very significant when it comes to wideband antennas. Exciting antenna in a single mode gives a narrowband performance, whereas the excitation of multiple modes results in wider bandwidth [15]. Characteristics mode analysis is a tool that predicts a material's natural resonance frequency without any feed information [16]. Characteristics mode analysis helps choose the appropriate feed location based on current distribution. A notch at the ground plane helps match the antenna impedance over a wider frequency range by extending the electrical length of the ground plane [16]. Fractal being a self-similar structure, an affine transformation with Iterated Function system can be used to build any self-replicating fractal structure.

This work proposes a novel miniaturized fractal antenna for IoT applications. Parametric and modal optimization resulted in a wider bandwidth. Optimizing the design with the help of characteristics mode analysis eliminated a stopband blocking the important IoT frequencies. The Smith chart-based optimization helped to concentrate the Z curve near the constant Γ circle yielding a wider bandwidth. The novelty of the design lies in its unique structure and stopband elimination to obtain wider bandwidth to cover all the IoT frequencies with a single antenna. The size reduction of the antenna while improving its performance is also a significant contribution to this work. The following sections constitute the paper. Section 1 proposes the antenna design procedure. Section 2 focuses on the parametric study. Section 3 provides antenna optimization to eliminate the stopband, and Section 4 discusses experimented results. Finally, the work concludes with a discussion of the proposed design's applicability in various IoT applications.

2. ANTENNA GEOMETRY

The design considers a fractal antenna considering the square microstrip patch of 27 mm × 27 mm as an initiator. Iteration I proceeds by dividing an initiator into nine equal squares of 9 mm × 9 mm each and then removing the two extreme squares in the direction of the left diagonal resulting in 7 squares of 9 mm × 9 mm in iteration I. Table 1 clearly illustrates the process. The steps have been repeated till iteration III. The geometry uses an FR4 substrate with a dielectric constant of 4.4 and substrate height of 1.6 mm. A line feed ensures the simplicity of the feeding. Table 1 visually explains the procedure involved in the geometry creation. Expression (1) reveals the fractal dimension. The scaling factor is three as each edge is divided into three equal parts.

$$D = \frac{\log(\text{number of copies of initiator})}{\log(\text{scaling factor})} = \frac{\log(7)}{\log(3)} = 1.77 \tag{1}$$

The steps involved in geometry are:

Refer to Table 1 Row I for Iteration I

Step 1: Take a square patch of 27 mm × 27 mm and divide it into nine squares of 9 mm × 9 mm each.

Step 2: Select the two extreme left diagonal squares (Highlighted in black color).

Step 3: Remove the two selected extreme left diagonal squares to get Iteration I.

Refer to Table 1 Row II for Iteration II

Step 4: Take the geometry designed in step 3 and divide it into squares of 3 mm × 3 mm each.

Table 1. Steps in geometry generation.

ITERATION I		
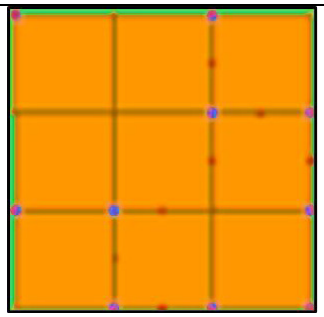	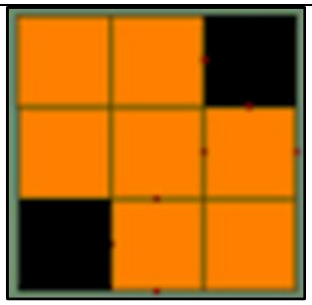	
Step 1: Divide 27 mm × 27 mm square in to 9 mm × 9 mm	**Step 2: Select the two extreme left diagonal squares**	**Step 3: Remove the two selected extreme left diagonal squares**
ITERATION II		
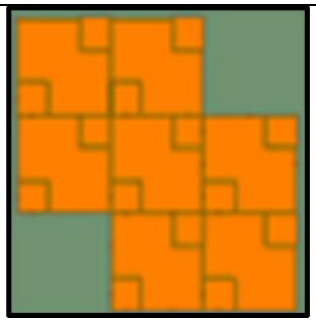	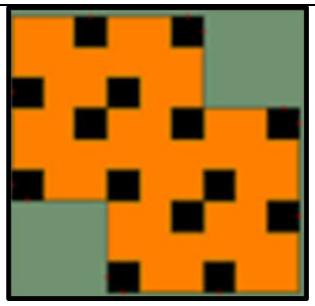	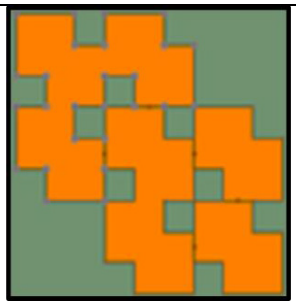
Step 4: Divide 9 mm × 9 mm square in to 3 mm × 3 mm	**Step 5: Select the extreme left diagonal squares**	**Step 6: Remove the selected extreme left diagonal squares**
ITERATION III		
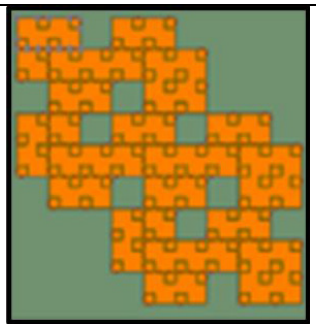	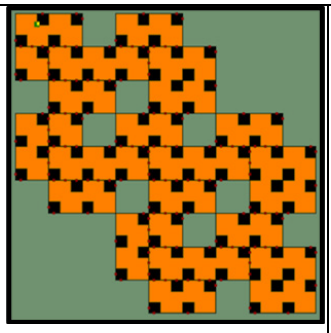	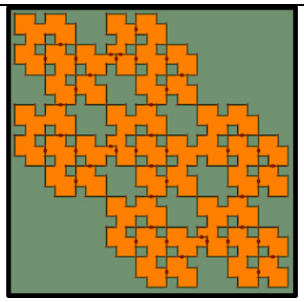
Step 7: Divide 3 mm × 3 mm square in to 1 mm × 1 mm	**Step 8: Select the extreme left diagonal squares**	**Step 9: Remove the selected extreme left diagonal squares**

Step 5: Select extreme left diagonal squares of 3 mm × 3 mm in a square of 9 mm × 9 mm square.

Step 6: Remove the selected extreme left diagonal squares of 3 mm × 3 mm in squares of 9 mm × 9 mm (Highlighted in black color) to get Iteration II.

Refer to Table 1 Row III for Iteration III

Step 7: Take the geometry designed in step 6, which has squares of 3 mm × 3 mm each; divide these 3 mm × 3 mm squares into 1 mm × 1 mm squares.

Step 8: Select only extreme left diagonal squares of 1 mm × 1 mm in a square of 3 mm × 3 mm.

Step 9: Remove the selected extreme left diagonal squares of 1 mm × 1 mm in squares of 3 mm × 3 mm (Highlighted in black color) to get Iteration III.

3. PARAMETRIC STUDY

A parametric study has been performed on the ground plane. A slot is inserted at the partial ground plane to experiment with the matching over a wider band. Figure 1 shows the different steps in which the parametric study has been performed. Starting from the whole ground plane (same as substrate dimensions) in Figure 2(a), then the partial ground plane in Figure 2(b), and the next steps, the notch dimensions have been varied to see its impact on impedance Figures 2(c)–(f). A notch at the ground plane helped match the antenna impedance over wider bandwidth by concentrating current towards the feed location. A proper choice of the partial ground plane, the dimensions of the notch in the ground plane, and the feed location helped match the antenna over a wider frequency. The partial ground plane and the notch control the impedance, whereas the feed location controls the resonance point.

Since the antenna size is minimal in the entire ground plane, its natural resonant point lies beyond 7 GHz. Therefore, it does not cover primary IoT frequencies, as depicted by the brown colored curve in Figure 3. Upon converting the whole ground to partial ground and fine-tuning the feed location, the

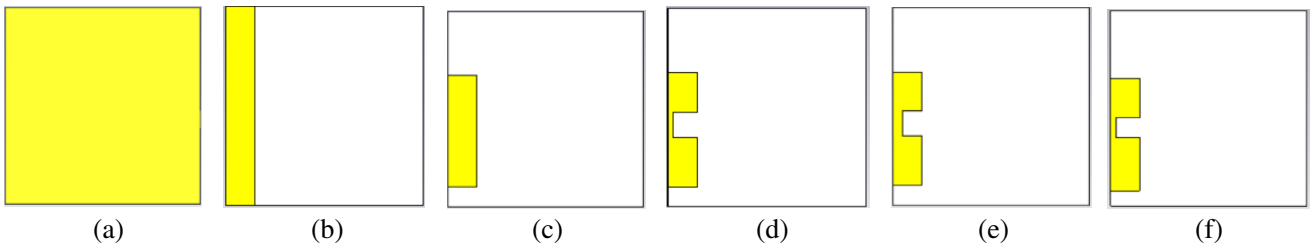

Figure 2. Parametric study. (a) Full ground, (b) partial ground, (c) partial defected ground, (d) 4 mm × 5 mm notch in the ground, (e) 5 mm × 4 mm notch in the ground, (f) 5 mm × 5 mm notch in the ground.

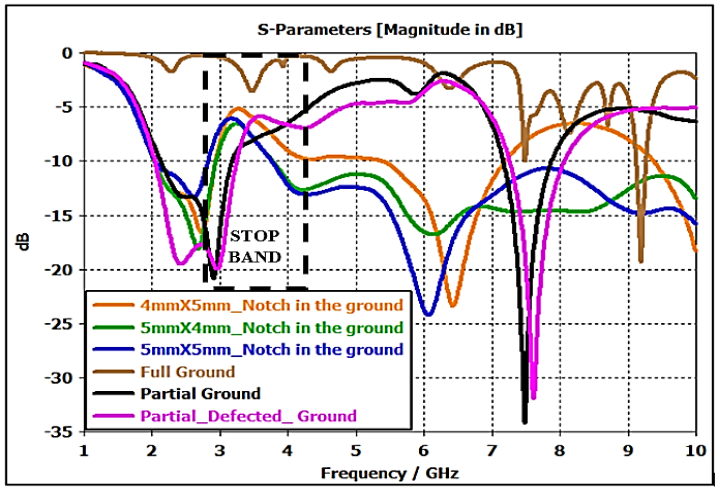

Figure 3. Parametric study of Iteration III showing green curve covering major IoT bands and a stop band at 3 GHz to 4 GHz.

resonance shifts towards the lower band covering 2 GHz–3 GHz and 7 GHz–8 GHz band (pink colored curve in Figure 3). Because fractal antennas have the potential to resonate over wider bandwidths, an attempt has been made not to alter the fractal surface in the parametric study. Therefore, a notch is inserted in the ground plane to increase the electrical length of the ground plane in order to investigate the wideband possibility. The notch location is chosen near the feed point so that the accelerated charges are dense near the feed location, causing the constant impedance on wider frequencies, resulting in resonance over a wide bandwidth. When The notch length × width is 4 mm × 5 mm, the band between 4 GHz and 7 GHz shows the possibility of broader bandwidth (orange colored curve in Figure 3). When the notch dimension is 5 mm × 4 mm, the S_{11} graph (Green curve in Figure 3) shows a broader band from 4 GHz to 13 GHz.

Further, when notch dimensions are 5 mm × 5 mm (blue curve in Figure 3), the S_{11} shows wider bandwidth between 4 GHz and 13 GHz. However, the performance deteriorated in the lower band, 2 GHz to 3 GHz (blue curve in Figure 3). As a result, the notch dimensions of 5 mm and 4 mm were chosen (green curve in Figure 3). Looking at the green curve in Figure 3, it is clear that, although this combination covers 2 GHz to 3 GHz and 4 GHz to 12 GHz, the stopbands between 3 GHz and 4 GHz exclude the significant IoT frequencies between 3 GHz and 4 GHz. Considering this, the antenna's geometry is optimized to improve the performance in 3 GHz and 4 GHz bands, as shown in the following section. The same parametric steps apply to Iteration II and Iteration III.

4. GEOMETRY OPTIMIZATION

A modal study eliminates the stopband between 3 and 4 GHz to find the modes operating at different frequencies, as shown in Figure 4. The characteristics angle in Figure 4(a) shows that no mode is crossing 180° in the band 3 GHz to 4 GHz; this justifies the reason behind the stopband. The current distribution responsible for the resonance at 3 GHz to 4 GHz is marked in a black circle in Figure 5. Figure 5 depicts three major regions responsible for the resonance at 3 and 4 GHz (b); these regions are optimized in 3 stages, as depicted in Figure 6. Figure 4(b) indicates the characteristics angle after optimization. In Figure 4(b), it is clear that mode 1 and mode 2, which are overlapping before optimization, are separated and shifted towards the 3 GHz–4 GHz band generating an additional resonance that lead to the elimination of the stopband.

The Smith chart in Figure 7(a) is more inclined towards the lower semicircle, where the capacitive reactance is optimal. To compensate for the impedance mismatch caused by increased capacitive reactance in Figure 7(a), regions I, II, and III are loaded with metal to shift the impedance circle

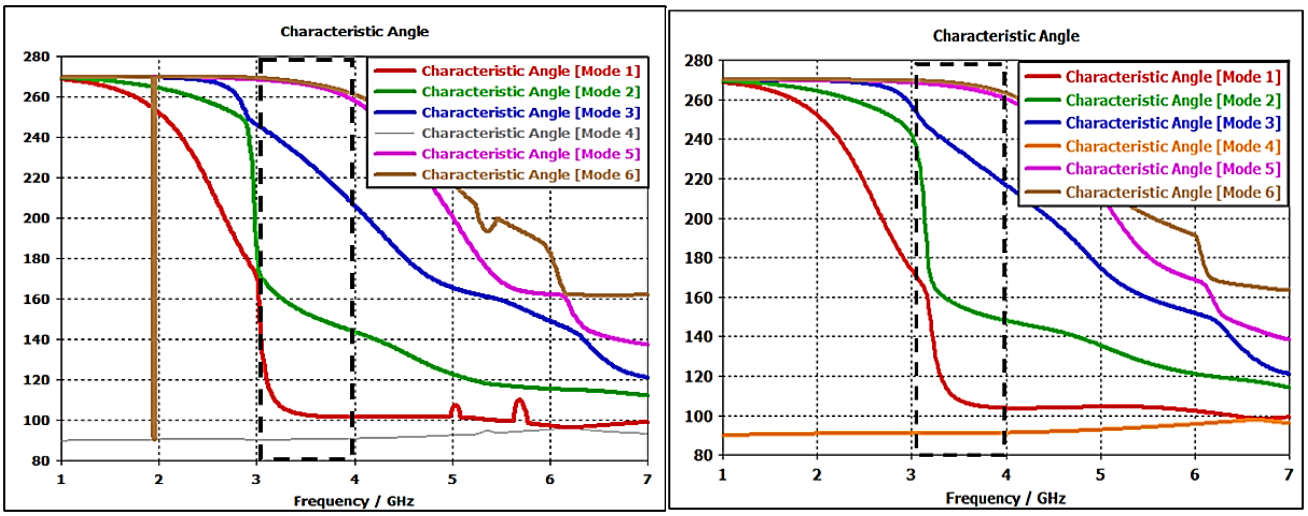

Figure 4. (a) Characteristics angle before optimization. (b) Characteristics angle after optimization.

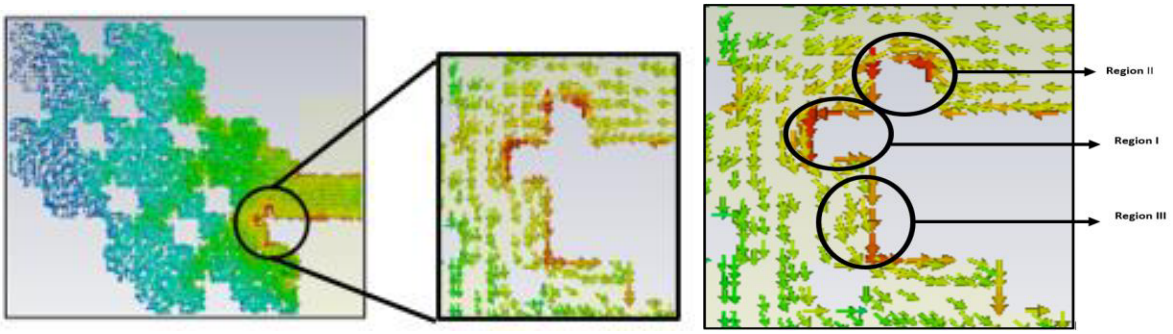

Figure 5. Region responsible for resonance at 3 GHz to 4 GHz.

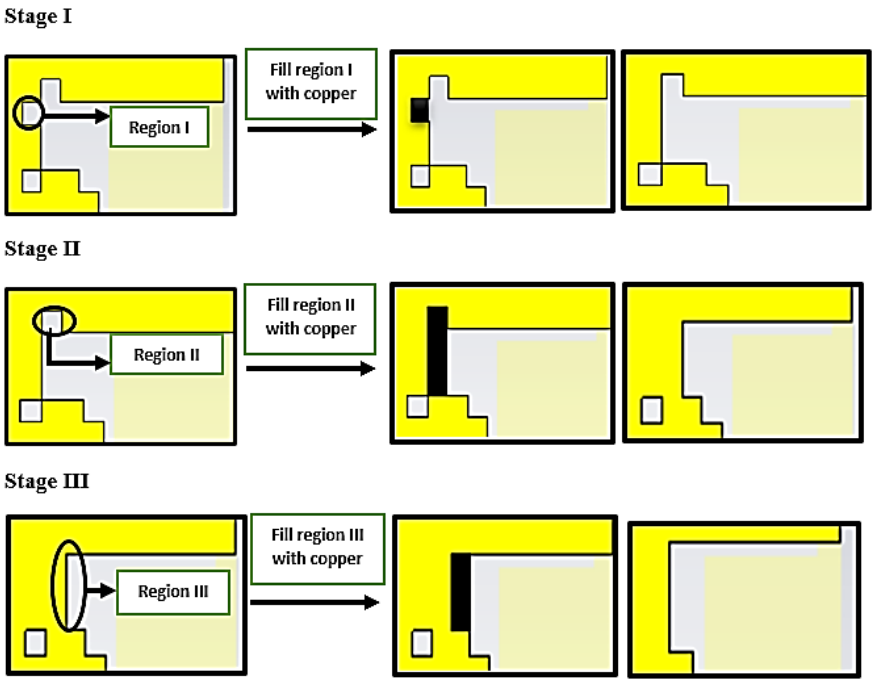

Figure 6. Stages in the optimization of Iteration III to eliminate stop band.

towards the inductive side (upper semicircle), as shown in Figure 6. Figure 6 depicts the stages of geometry optimization. Region I is filled with metal during stage I. Region II is filled with metal in stage II, and Region III is filled with metal in stage III. With each optimization stage, the impedance curve increasingly converges towards a constant Γ circle, as shown in Figures 7(b)–(d), and the stopband is reduced. To learn more about the Smith chart, readers may refer to [18].

Figure 7(d) shows how Z_{11} is converged near the constant Γ circle, thus eliminating the stopband successfully. Figure 8 shows the geometry transformation in each stage of optimization. While performing optimization, care has been taken to avoid destroying the basic structure of the proposed fractal, as indicated by the black circle. Figure 9(a) indicates how Z_{11} matches with successive optimization stages. Figure 9(b) shows the voltage standing wave ratio (VSWR) below 3 in the desired band, indicating the match between the antenna and input port. Mode 1 and mode 2, which degenerate at 180° before optimization, are separated after optimization producing an additional resonance in the 3 GHz to 4 GHz band as shown in Figure 4(b).

The S_{11} in Figure 10 shows how the stopband is reduced in each stage of optimization covering the major IoT frequencies from 2 GHz to 7 GHz.

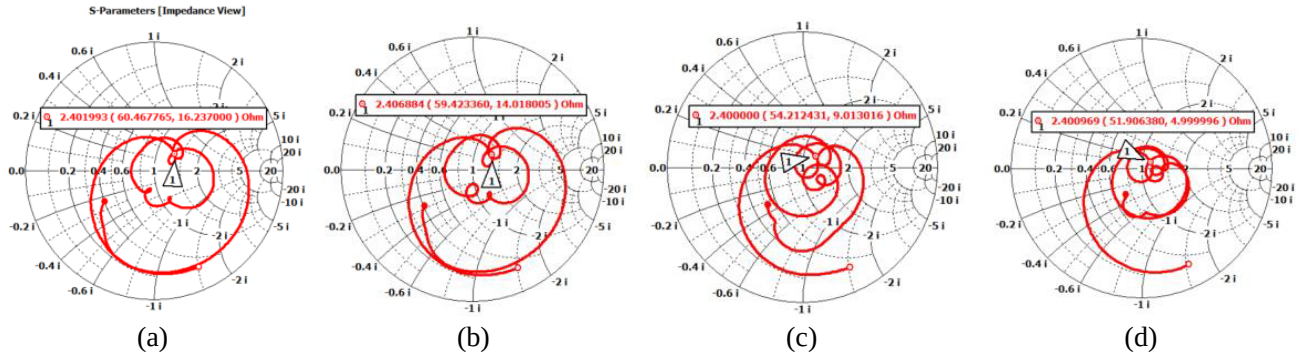

Figure 7. Z_{11} transition with each stage of optimization. (a) Unoptimized Z_{11}, (b) Stage-I, Z_{11}, (c) Stage-II, Z_{11}, (d) Stage-III Z_{11}.

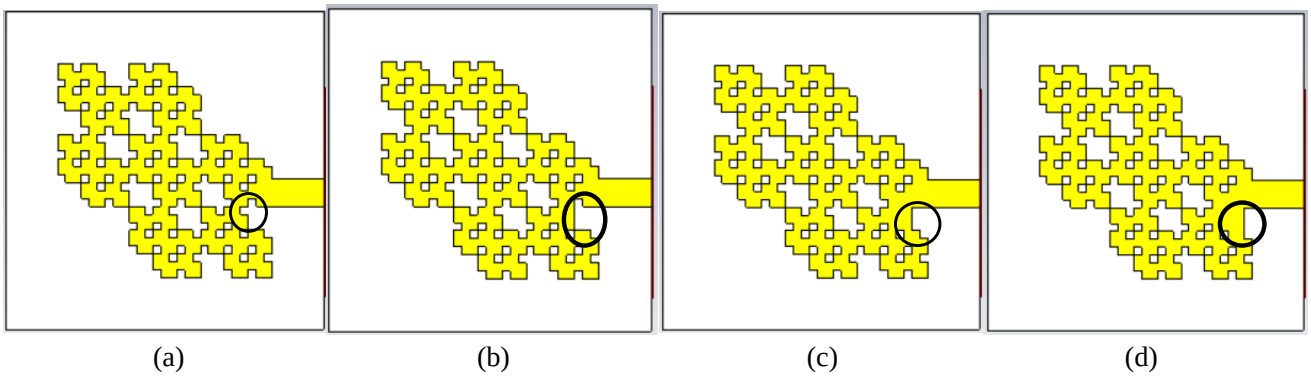

Figure 8. Z_{11} transition with each stage of optimization. (a) Unoptimized geometry, (b) Stage-I geometry, (c) Stage-II, geometry, (d) Stage-III geometry.

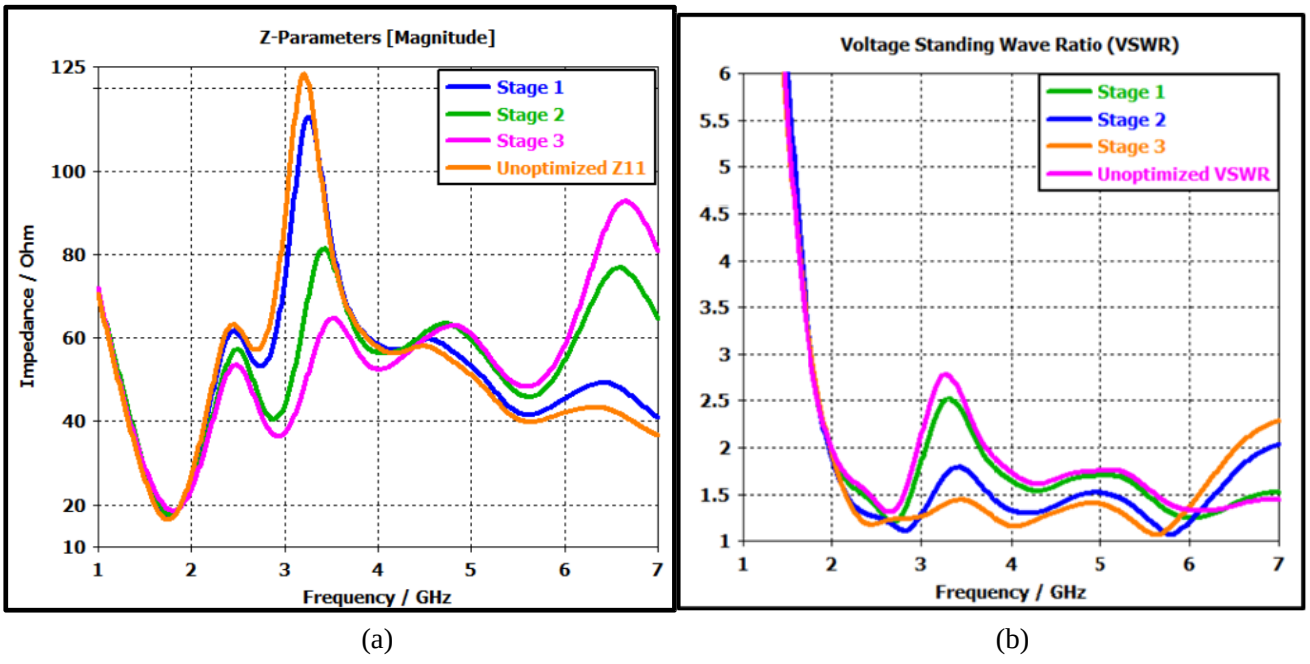

Figure 9. (a) Z_{11} with each stage of optimization. (b) VSWR with each stage of optimization.

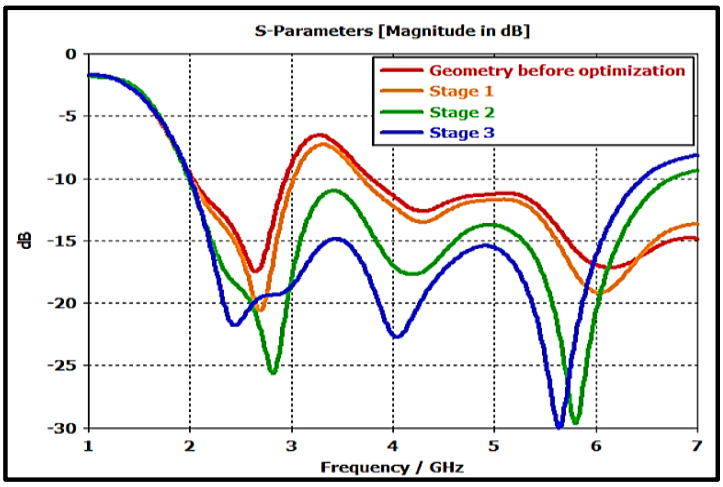

Figure 10. Stepwise improvement in S_{11} with optimization in stage I, Stage II and Stage III.

5. DISCUSSION ON RESULTS

Iteration II:

Iterations II and III have been fabricated (Figure 11 and Figure 13) to observe the antenna's behavior in real-time. The design has been tested with the help of a vector network analyzer and an anechoic chamber. Iteration II resonates from frequency 2.4 GHz to 3.5 GHz with an S_{11} of -40 at

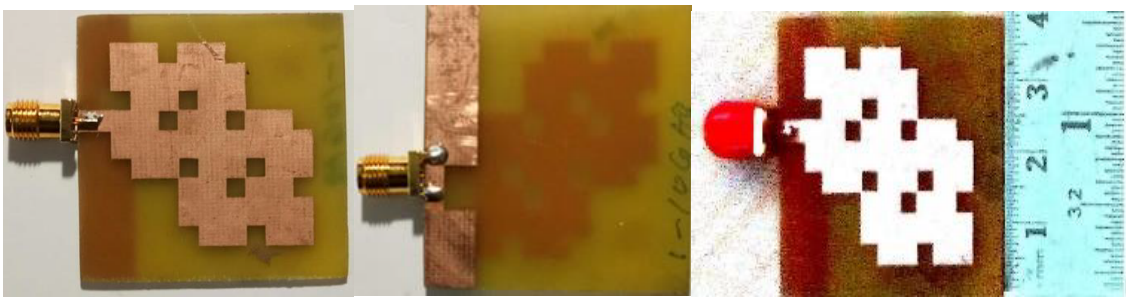

(a) (b) (c)

Figure 11. Fabricated prototype of Iteration II geometry. (a) Front view. (b) Back view. (c) Overall size.

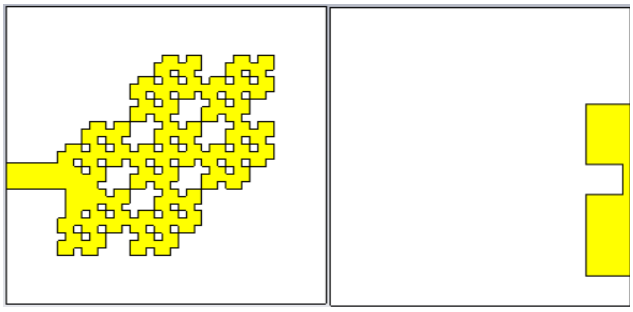

Figure 12. Iteration III in CST Studio.

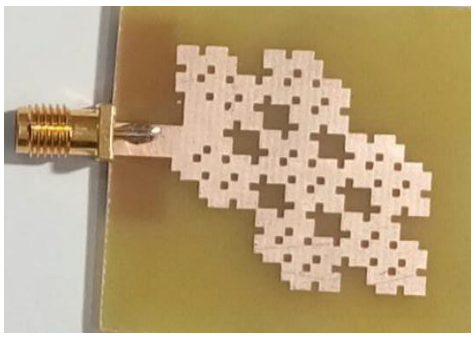

Figure 13. Fabricated prototype of Iteration III.

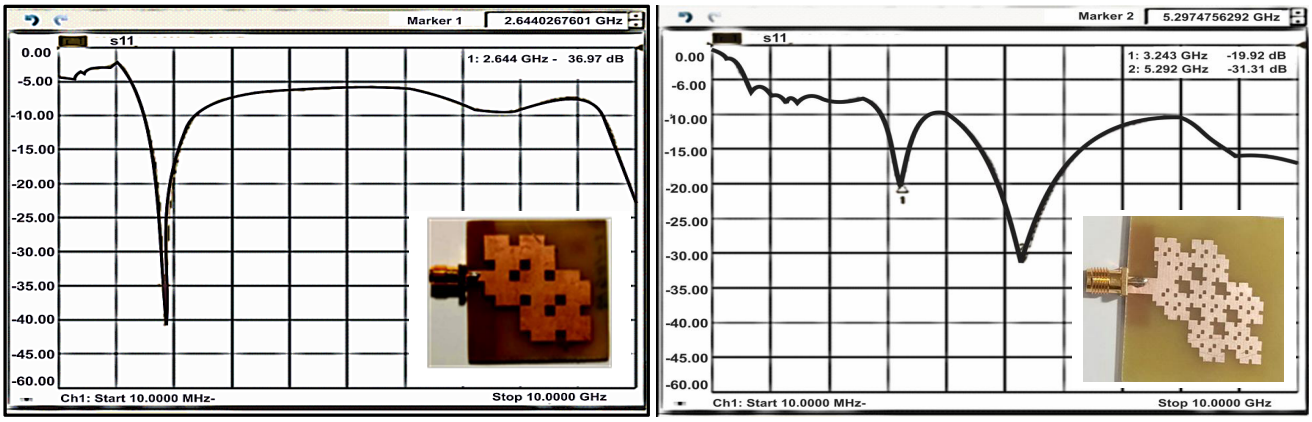

(a) (b)

Figure 14. (a) Measured S_{11} of Iteration II. (b) S_{11} of Iteration III.

2.6 GHz, as depicted in Figure 14(a). The geometry has been fabricated on an FR4 substrate with a height of 1.6 mm. The overall size of Iteration II is 40 mm × 40 mm × 1.6 mm, as depicted in Figure 11(c), with a partial ground and a notch in the ground plane as indicated in Figure 11(a) and Figure 11(b). The measured VSWR at the resonance of Iteration II is below two, indicating that the structure is perfectly matched to the feed, as given in Figure 15(a).

Iteration III:

In Iteration III, the geometry has been optimized over a wider band of frequencies by optimizing a ground plane and eliminating the stopband between 3 and 4 GHz, as discussed in the previous sections. The optimized geometry of Iteration III is shown in Figure 12. The fabricated prototype of Iteration III is given in Figure 13. As a result of stopband elimination, the antenna at Iteration III resonates over a wider band from 2 GHz to 7 GHz, covering all the frequencies for IoT applications, as illustrated in Figure 14(b). In addition, the measured VSWR plot of Iteration III in Figure 15(b) shows a good matching between the port and antenna responsible for wideband performance.

An important factor that quantifies antenna bandwidth and miniaturization is the Bandwidth Dimension Ratio (BDR) [17]. A BDR of 203.44 is calculated with the formula given in Equations (2),

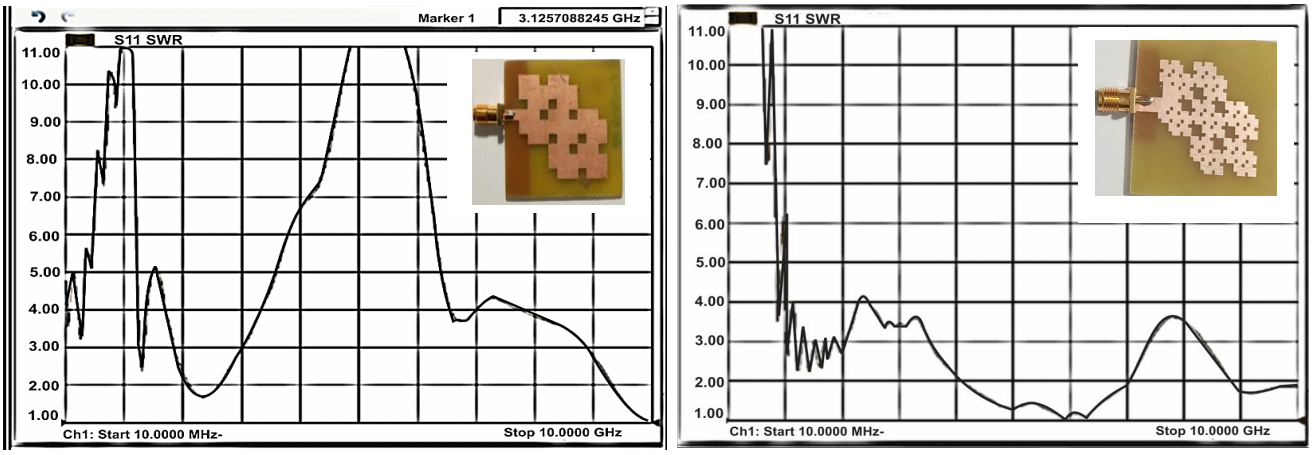

(a) (b)

Figure 15. (a) VSWR of Iteration II. (b) VSWR of Iteration III.

(3), and (4).

$$\text{BDR} = \frac{\text{BW\%}}{\lambda_l * \lambda_W} \tag{2}$$

$$\lambda_l = \frac{L_g}{\lambda_0} \tag{3}$$

$$\lambda_W = \frac{W_g}{\lambda_0} \tag{4}$$

L_g and W_g are electrical length and width of ground plane and $\lambda_0 = \frac{C}{f_c}$; C is the speed of light in free space; f_c is the centre frequency.

The surface current path is increased due to the fractal structure in the developed antenna, increasing the electrical length of the antenna. As a result, the overall surface of an antenna with the same resonance frequency is significantly reduced. In addition, this method results in a patch size reduction.

6. COMPARISON WITH RECENT LITERATURES

The proposed design is compared with the recent literature, as the substrate material greatly influences the antenna behavior. The design is compared with the designs using an FR4 substrate for the design. Size reduction and bandwidth improvement are two major criteria for comparison, as can be seen in Table 2. The proposed design performs better than the references mentioned in the table. However, better-performing antennas exist in the recent literature, like in [17]. Furthermore, the proposed geometry still has the potential to extend its bandwidth which can be taken as future work.

Table 2. Comparison with recent literatures.

Reference	Antenna Size	Substrate Material	Bandwidth
[11]	50 mm × 60 mm × 1.6 mm	FR4	27 to 33 GHz
[12]	70 mm × 60 mm × 1.5 mm	FR4	1.3–3.7 GHz
[13]	45 mm × 40 mm × 1.6 mm	FR4	3.79 GHz and 5.5 GHz
[14]	45 mm × 25 mm × 1.6 mm	FR4	4.94 GHz and 6.12 GHz
Proposed Antenna Iteration II	40 mm × 40 mm × 1.6 mm	FR4	2.4 GHz to 3.5 GHz
Proposed Antenna Iteration III	40 mm × 40 mm × 1.6 mm	FR4	2.0 GHz and 7.0 GHz

Figure 16 compares S_{11} of Iterations II and III from CST, Mentor Graphics, and measured results, highlighting the improved bandwidth in Iteration III. Figure 14(a) depicts S_{11} at Iteration II which is slightly poor because fewer fractal slots result in lower λ and less path for current distribution. As a result, the geometry is not optimized in Iteration II. However, Iteration II may also result in an enhanced bandwidth and S_{11} if the Smith chart-based optimization is applied. As the final iteration (Iteration III) is considered for fabrication, Iteration III is optimized, and Iteration II is reported as unoptimized geometry. Reflections caused by sharp corners of fractal slots cause a slight shift in the simulated and measured results. Figure 17 depicts the simulated and measured gains, with Iteration III reporting a peak gain of up to 4.5 dBi. Figure 18 depicts a nearly oval-shaped radiation pattern at lower frequencies that are slightly distorted at higher frequencies due to the excitation of higher-order modes.

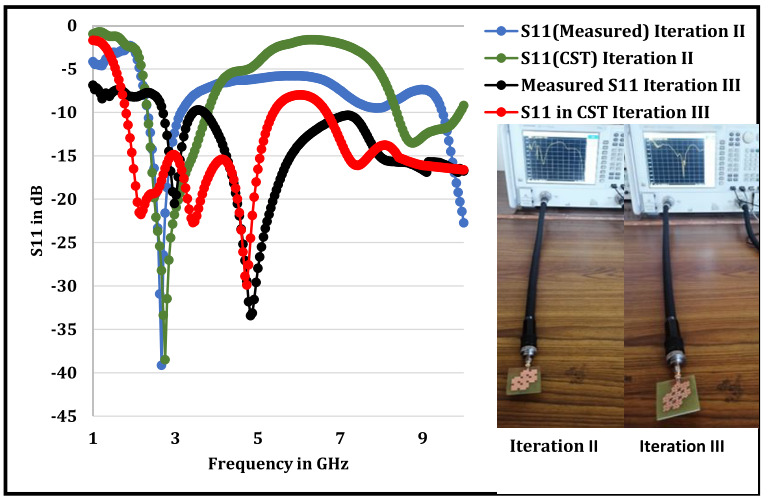

Figure 16. S_{11} comparison of Iteration II and Iteration III.

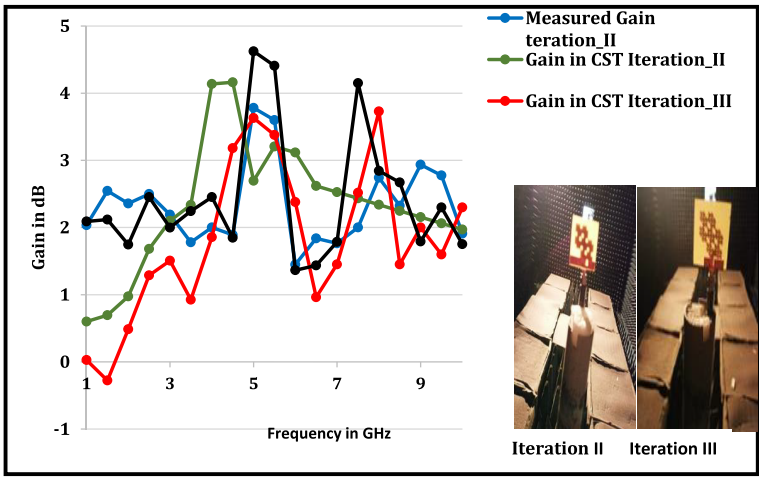

Figure 17. Gain comparison of Iteration II and Iteration III.

7. EFFECTIVENESS OF PROPOSED OPTIMIZATION TECHNIQUE WITH GENETIC ALGORITHM (GA), PARTICLE SWARM OPTIMIZATION (PSO), DIFFERENTIAL EVOLUTION (DE)

The No Free Lunch (NFL) theorem guarantees that the best global optimizer does not exist [19]. Nevertheless, optimization methods such as Genetic Algorithm (GA), Particle Swarm Optimization (PSO), and Differential Evolution (DE) are effective in solving specific antenna design problems. The search for new algorithms and their application to antenna design problems is an ongoing research process that will likely continue indefinitely. Although GE, PSO, and DE provide multi-objective optimization, the coding is complex, and many people still prefer the weighted sum single-objective optimization approach for various optimization case studies.

Maintaining a proper balance of population diversity and selection pressure (crossover probability, mutation probability, population size, and the maximum number of generations) is challenging in Genetic Algorithm-based optimization techniques [20]. The presence of $\begin{pmatrix} 0 & 1 \\ 1 & 0 \end{pmatrix}$, $\begin{pmatrix} 1 & 0 \\ 0 & 1 \end{pmatrix}$ constellation, where two sub-patches touch at the corner, is a problem with antenna design in GA.

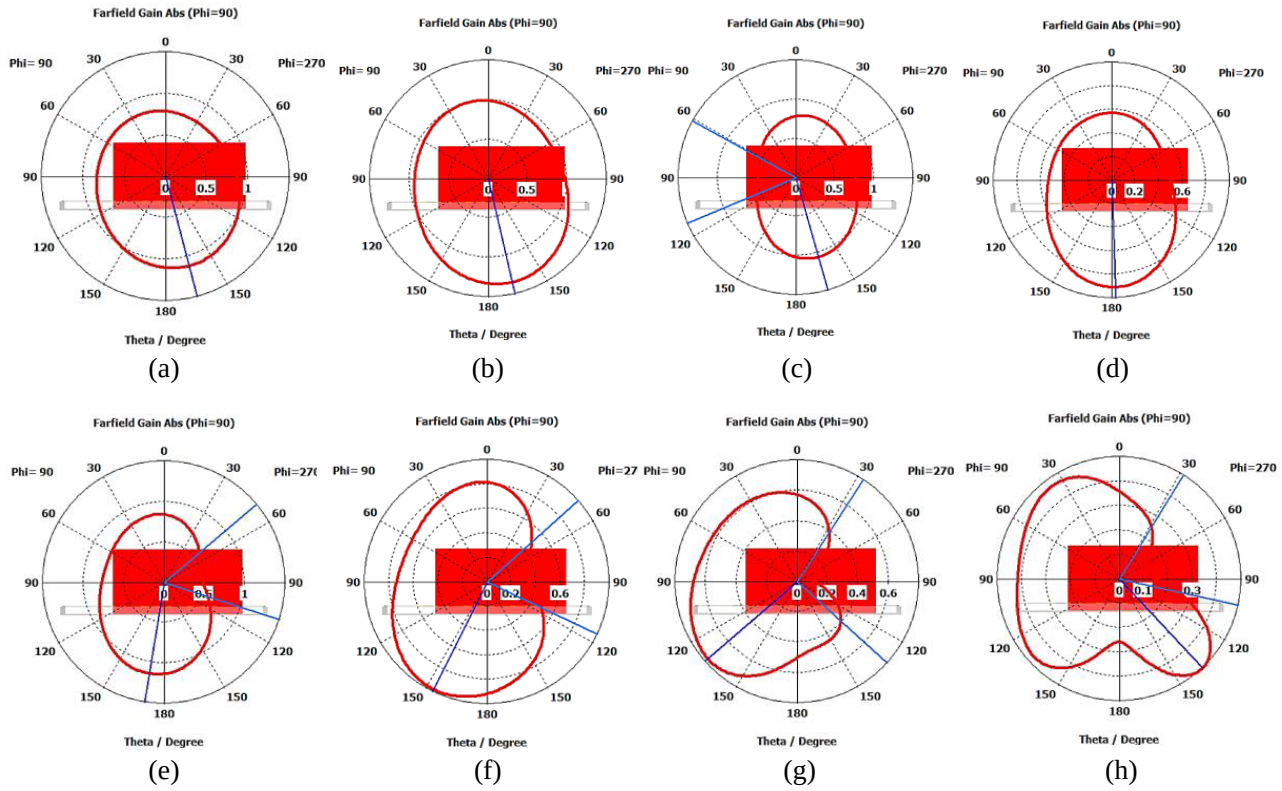

Figure 18. Radiation pattern of Iteration III at different frequencies. (a) 2 GHz, (b) 2.4 GHz, (c) 3.6 GHz, (d) 4 GHz, (e) 4.5 GHz, (f) 5 GHz, (g) 5.5 GHz, (h) 6 GHz.

This may cause a problem when fabricating the microstrip fractal antenna [21]. In PSO, more search space exploration needs to be ensured for reduced chances of local minima trapping at the expense of increased computational cost and slower speed; however, PSO is time economic compared to the GA [22]. A comparison of GA, PSO, and DE is reported in [19]. Premature convergence and search efficiency are the two major concerns in differential evolution algorithms [23].

GA, PSO, and DE are effective in optimizing multi-antenna problems such as arrays. When these algorithms are applied to single antenna problems, the optimized geometry may have a random structure and provide less physical insights into the electromagnetic behavior of the antenna. On the other hand, the proposed optimization method targets only the impacted region based on the current distribution and analysis of the optimization effects at every step with the help of a Smith chart. The proposed method is flexible and need not require complex programming skills; however, the algorithm can be programmed for complex antenna problems. The proposed optimization technique retains the original structural properties of the antenna. The time required for optimization is almost equal to the time required for electromagnetic simulation. The proposed optimization technique is flexible and may be clubbed with traditional optimization algorithms for enhanced performance in electromagnetic-related problems.

8. CONCLUSION

The proposed antenna resonates in the frequency band of 2 GHz to 7 GHz, covering 2.4 GHz (Z-wave, Bluetooth) Wi-Fi (2.4 GHz, 3.6 GHz, 4.9 GHz, 5 GHz, 5.9 GHz), Wireless HART (2.4 GHz), ISA 100.11A 2.4 GHz, MBAN (2360–2400 MHz), WBAN (2.4 GHz), WAIC 4200–4400 MHz. The antenna is suitable for general (smart home and commercial applications), IoT, medical, and avionics applications. A surface current distribution-based stopband elimination technique helped to cover all the IoT bands by reducing the stopband. Characteristic mode analysis helped in understanding the modal behavior

while optimizing the design. A notch at the partial ground facilitated the impedance match over more comprehensive frequencies. An appropriate choice of feed location, notch dimensions, and partial ground dimensions helps optimize the geometry over a wider band without deteriorating the original structure of the fractal.

REFERENCES

1. Mohanty, M. N., S. Satrusallya, and T. Al Smadi, "Antenna selection criteria and parameters for IoT application," *Printed Antennas Design and Challenges*, 1st Edition, CRC Press, 2023.
2. Balanis, C. A., *Antenna Theory: Analysis and Design*, 4th Edition, Wiley, 2016.
3. Khan, U. R., J. A. Sheikh, A. Junaid, R. Amin, S. Ashraf, and S. Ahmed, "Design of a compact hybrid Moore's fractal inspired wearable antenna for IoT enabled bio-telemetry in diagnostic health monitoring system," *IEEE Access*, Vol. 10, 116129–116140, 2022, doi: 10.1109/ACCESS.2022.3219442.
4. Puente, C., J. Romeu, R. Pous, X. Garcia, and F. Benitez, "Fractal multiband antenna based on the Sierpinski gasket," *Electronics Letters*, Vol. 32, No. 1, 1–2, 1996.
5. Parker, E. A. and A. N. A. El Sheikh, "Convoluted array elements and reduced size unit cells for frequency-selective surfaces," *IEE Proceedings. Part H*, Vol. 1, 19–22, 1991.
6. Sediq, H. T., J. Nourinia, C. Ghobadi, and B. Mohammadi, "A novel shaped ultrawideband fractal antenna for medical purposes," *Biomedical Signal Processing and Control*, Vol. 80, Part 2, 104363, February 2023, https://doi.org/10.1016/j.bspc.2022.104363.
7. Mohanty, A. and S. Sahu, "2-D printed 8-element compact UWB diversity antenna for multi-service-multi-mode applications," *International Journal of Electronics and Communications*, Vol. 151, 154215, July 2022, https://doi.org/10.1016/j.aeue.2022.154215.
8. Mohanty, A. and S. Sahu, "Design of 8-port compact hybrid fractal UWB MIMO antenna with a conjoined reflector-ground integration for isolation improvement," *International Journal of Electronics and Communications*, Vol. 145, 154102, February 2022, https://doi.org/10.1016/j.aeue.2021.154102.
9. Sree, G. N. J. and S. Nelaturi, "Design and experimental verification of fractal based MIMO antenna for lower sub 6-GHz 5G applications," *International Journal of Electronics and Communications*, Vol. 137, 153797, July 2021, https://doi.org/10.1016/j.aeue.2021.153797.
10. Baqira, M. A., H. Latifa, O. Altintas, M. N. Akhtar, M. Karaaslan, H. Servera, M. Hameed, and N. M. Idreesd, "Fractal metamaterial based multiband absorber operating in 5G regime," *Optik*, Vol. 266, 169626, September 2022, https://doi.org/10.1016/j.ijleo.2022.169626.
11. Karanam, R. and D. Kakkar, "Artificial neural network optimized ultra wide band fractal antenna for vehicular communication applications," *Transactions on Emerging Telecommunications Technologies*, Vol. 33, No. 12, e4620, 2022, https://doi.org/10.1002/ett.4620.
12. Alqahtani, A., M. T. Islam, M. S. Talukder, M. Samsuzzaman, M. Bakouri, S. Mansouri, T. Almoneef, S. Dokos, and Y. Alharbi, "Slotted monopole patch antenna for microwave-based head imaging applications," *Sensors*, Vol. 22, 7235, 2022, https://doi.org/10.3390/s22197235.
13. Desai, A., T. K. Upadhyaya, R. Patel, S. Bhatt, and P. Mankodi, "Wideband high gain fractal antenna for wireless applications," *Progress In Electromagnetics Research Letters*, Vol. 74, 125–130, 2018.
14. Jamil, A., M. Rauf, A. Sami, A. Ansari, and M. D. Idrees, "A wideband hybrid fractal ring antenna for WLAN applications," *International Journal of Antennas and Propagation*, Vol. 2022, Article ID 6136916, 8 pages, Hindawi, 2022, https://doi.org/10.1155/2022/6136916.
15. Strojny, B. T., "Excitation and analysis of characteristic modes on complex antenna structures," The Ohio State University, 2011.
16. Kalkhambkar, G. B., R. Khanai, and P. Chindhi, "Design and characteristics mode analysis of a cantor set fractal monopole antenna for IoT applications," *Progress In Electromagnetics Research C*, Vol. 119, 161–175, 2022.

17. Sagne, D. and R. A. Pandhare, "Design and analysis of inscribed fractal super wideband antenna for microwave applications," *Progress In Electromagnetics Research C*, Vol. 121, 49–63, 2022.
18. https://coppermountaintech.com/help-s4/smith-chart-format.html.
19. Goudos, S. K., C. Kalialakis, and R. Mittra, "Evolutionary algorithms applied to antennas and propagation: A review of state of the art," *International Journal of Antennas and Propagation*, 1–12, 2016, doi: 10.1155/2016/1010459.
20. Haupt, R. L., "An introduction to genetic algorithms for electromagnetics," *IEEE Antennas and Propagation Magazine*, Vol. 37, No. 2, 7–15, 1995, doi: 10.1109/74.382334.
21. Lamsalli, M., A. El Hamichi, M. Boussouis, N. A. Touhami, and T. Elhamadi, "Genetic algorithm optimization for microstrip patch antenna miniaturization," *Progress In Electromagnetics Research Letters*, Vol. 60, 113–120, 2016.
22. Lim, S. P. and H. Haron, "Performance comparison of genetic algorithm, differential evolution and particle swarm optimization towards benchmark functions," *2013 IEEE Conference on Open Systems (ICOS)*, 41–46, Kuching, Malaysia, 2013, doi: 10.1109/icos.2013.6735045.
23. Liu, H., C.-Y. Yin, and W.-D. Gao, "Optimization and design of wideband antenna with adaptive differential evolution algorithm based on dual population," *IEEE 2015 Asia-Pacific Microwave Conference (APMC)*, 1–3, Nanjing, China, 2015, doi: 10.1109/apmc.2015.7413230.